First-principles study of intermediate-spin ferrous iron in the Earth's lower mantle

Han Hsu[1,*] and Renata M. Wentzcovitch[2,3,†]

[1]*Department of Physics, National Central University, Jhongli City, Taoyuan 32001, Taiwan*
[2]*Department of Chemical Engineering and Materials Science, University of Minnesota, Minneapolis, Minnesota 55455, USA*
[3]*Minnesota Supercomputing Institute, University of Minnesota, Minneapolis, Minnesota 55455, USA*

Spin crossover of iron is of central importance in solid Earth geophysics. It impacts all physical properties of minerals that altogether constitute ~ 95 vol% of the Earth's lower mantle: ferropericlase [(Mg,Fe)O] and Fe-bearing magnesium silicate (MgSiO$_3$) perovskite. Despite great strides made in the past decade, the existence of an intermediate-spin (IS) state in ferrous iron (Fe^{2+}) (with total electron spin $S = 1$) and its possible role in the pressure-induced spin crossover in these lower-mantle minerals still remain controversial. Using density functional theory + self-consistent Hubbard U (DFT + U_{sc}) calculations, we investigate all possible types of IS states of Fe^{2+} in (Mg,Fe)O and (Mg,Fe)SiO$_3$ perovskite. Among the possible IS states in these minerals, the most probable IS state has an electronic configuration that significantly reduces the electron overlap and the iron nuclear quadrupole splitting (QS). These most probable IS states, however, are still energetically disfavored, and their QSs are inconsistent with Mössbauer spectra. We therefore conclude that IS Fe^{2+} is highly unlikely in the Earth's lower mantle.

PACS number(s): 75.30.Wx, 71.15.Mb, 71.20.Be, 91.60.Gf

I. INTRODUCTION

Spin crossover, a phenomenon of interdisciplinary interest, can occur in various length scales, including molecules (coordination complexes or coordination compounds), epitaxial thin films, and bulk solids. Transition-metal ions with four to seven d electrons (d^4–d^7 ions) contained in these systems can undergo a change of total electron spin (S) induced by extraneous factors, such as temperature, pressure, strain, chemical doping, or electromagnetic fields. Among the known spin-crossover systems, the Earth's lower mantle is the largest. Located 660–2890 km deep, this region of the Earth interior has a wide pressure (P) and temperature (T) range, spanning over 23–135 GPa and 1900–4000 K, respectively. The lower mantle is dominated by iron-bearing minerals: ~ 20 vol% of ferropericlase (Fp) [(Mg,Fe)O], ~ 75 vol% of Fe-bearing magnesium silicate (MgSiO$_3$) perovskite (Fe-Pv), and a relatively thin layer of Fe-bearing MgSiO$_3$ postperovskite (Fe-Ppv) located in its bottom (D'' layer). Ever since the observation of spin crossover in Fp and Fe-Pv [1,2], the work on these minerals has risen to a new high, especially for Fp, due to its simple rocksalt structure. It is believed that Fe^{2+} in Fp undergoes a crossover from the high-spin (HS) state ($S = 2$) to the low-spin (LS) state ($S = 0$) between 40 and 70 GPa. This spin crossover directly affects the structural, elastic, thermodynamic, optical, and conducting properties of Fp [3–16]; it also affects iron diffusion and thus perhaps viscosity and iron partitioning in the Earth's interior [17–19]. Based on these findings, geophysical effects of spin crossover have been anticipated.

In contrast, spin crossover in Fe-Pv, the *major* lower-mantle mineral phase, has been highly controversial [20–34], due to the complex nature of this mineral. In addition to Fe^{2+} that substitutes Mg in the dodecahedral (A) site forming

(Mg,Fe)SiO$_3$ Pv, there is also ferric iron (Fe^{3+}) substituting both Mg and Si [residing in the octahedral (B) site], forming (Mg,Fe)(Si,Fe)O$_3$ Pv. With the recent findings made by first-principles calculations [32,33], a consensus has gradually been reached: Only Fe^{3+} residing in the B site undergoes a crossover from a HS ($S = 5/2$) to a LS ($S = 1/2$) state; iron in the A site remains in a HS state, regardless of its oxidation state. The geophysical consequences of spin crossover are still unclear, but its possible effects on mineral properties have been reviewed or summarized in literature [35–40]. More recently, it was found that Fe-Pv dissociates into Fe-free Pv and a hexagonal iron-rich silicate at conditions existing at approximately 2000 km depth and beyond [41]. The crystal structure and stability field of this hexagonal phase, however, have not been characterized yet. Therefore, it is important to properly characterize the state of iron at lower-mantle conditions, so the dissociation phase boundary in Fe-Pv can be better clarified.

While the spin crossovers in Fp and Fe-Pv are nearly understood, one issue still remains unresolved. As a d^6 ion, an intermediate-spin (IS) state with $S = 1$ is possible for Fe^{2+}. The existence of IS Fe^{2+} in Fp and (Mg,Fe)SiO$_3$ Pv, however, has not been *fully* confirmed nor excluded. For Fp, x-ray emission spectroscopy spectra show the total electron spin moment decreasing with pressure, as indicated by the decreasing satellite peak ($K\beta'$) intensity [1,3,8]. However, both the currently perceived HS-LS crossover or a more complicated HS-IS-LS crossover can lead to decreasing $K\beta'$. Also, while the change of iron nuclear quadrupole splitting (QS) observed in the Mössbauer spectra [4,5,11] indicates a change of d-electron configuration, it is insufficient to exclude or confirm an IS state. Recently, the existence of IS Fe^{2+} in Fp was investigated, but its possible role in spin crossover was not addressed [42]. As for (Mg,Fe)SiO$_3$ Pv, IS Fe^{2+} has been highly debated. An observed crossover from a lower QS (~ 2.4 mm/s) to a higher QS ($\geqslant 3.5$ mm/s) was suggested to be indicative of an HS-IS crossover, as the high QS was suggested to be a signature of IS Fe^{2+} [28]. Previous first-principles

———————
*hanhsu@ncu.edu.tw
†wentz002@umn.edu

calculations, however, showed that two distinct types of HS states with distinct QSs and one IS state are possible; it is the crossover between two HS states leading to the drastic change of QS, from 2.4 to 3.5 mm/s [32,33]. The one IS state, on the other hand, is energetically unfavorable; its QS obtained by calculation ($\leqslant 1.6$ mm/s) was not observed in experiments either [32,33]. So far, IS Fe^{2+} in Fe-Pv is still puzzling. One reason is the lack of a thorough knowledge of the IS Fe^{2+} reported in Ref. [32]; the other is the possibility of multiple types of IS Fe^{2+}. After all, Fe-Pv is known to have two distinct types of HS Fe^{2+}; it may have multiple types of IS Fe^{2+} as well. Recently, an anomalous conductivity change in Fe-Pv with increasing pressure was observed, and it was attributed to a possible HS-IS crossover of Fe^{2+} [34]. Given that the mechanism of spin crossover is usually deduced from an anomalous change in mineral properties *indirectly* related to iron's spin state, a comprehensive theoretical study for IS Fe^{2+} in Fp and Pv is highly desirable to clear this long-standing debate.

In addition to geophysics, the IS state in Fe^{2+} and other d^6 ions are of broad interest. Confirmation of IS Fe^{2+} in minerals can significantly change our current knowledge of the iron spin distribution (spin map) in the Earth, and an accurate spin map can be used to test theories beyond the standard model in particle physics [43]. A possible connection between IS Fe^{2+} and superconductivity in iron-based superconductors has been discussed but is still unclear [44–47]. IS Fe^{2+} would add versatility to the range of possibility of molecular devices based on coordination complexes/compounds [48], but its existence is still controversial (see, e.g., Ref. [49]) and conditions for its existence seem to be limited [50]. Last, but not least, the strain-induced ferromagnetic insulating state in lanthanum cobaltite ($LaCoO_3$) thin film and its possible relation with IS Co^{3+} has attracted significant attention and is still being debated [51–66]. A comprehensive theoretical study of IS Fe^{2+} in minerals with different atomic structures under increasing pressure can be expected to provide different perspectives for these problems.

II. COMPUTATION

In this work, all major calculations are performed using the local density approximation + self-consistent Hubbard U (LDA + U_{sc}) method, as LDA + U_{sc} gives the most accurate equation of states for iron-bearing Earth minerals and best predicts the occurrence and mechanism of spin crossover in them, compared with other functionals [32,33,39]. Structural optimizations for a 64-atom $(Mg_{1-x},Fe_x)O$ supercell ($x = 0.03125$) and a 40-atom $(Mg_{1-x},Fe_x)SiO_3$ supercell ($x = 0.125$) in all possible spin states are performed with variable cell shape molecular dynamics [67] implemented in the QUANTUM ESPRESSO code [68], which adopts the plane-wave pseudopotential method. Pseudopotentials used in this paper have been reported in Ref. [27] and used in other works regarding Earth minerals [27,32,33,39,40]. A $4 \times 4 \times 4$ **k**-point mesh is used for both Fp and Fe-Pv supercells. In this paper, we compute the Hubbard U for each spin state with a self-consistent procedure [33,69–71]; the resultant Hubbard U is referred to as self-consistent U (U_{sc}) hereafter. A detailed description of this procedure can be found in Ref. [33] and

its online Supplemental Material. In brief, we start with an LDA + U calculation with a trial U (U_{in}) to get all possible spin states. By applying local perturbations to the iron site in the LDA + U_{in} ground state with the Hubbard potential being held fixed, the second derivative of the LDA energy with respect to the electron occupation at the iron site can be obtained using a linear response theory [72]. This second derivative, U_{out}, will be used as U_{in} in the next iteration. Such a procedure is repeated until self-consistency is achieved, namely, $U_{in} = U_{out} \equiv U_{sc}$.

The iron nuclear quadrupole splitting (QS), ΔE_Q, of each possible spin state is computed using

$$\Delta E_Q = \frac{eQ|V_{zz}|}{2}\sqrt{1 + \frac{\eta^2}{3}}, \tag{1}$$

where e is electron charge, V_{zz} is the electric field gradient (EFG), η is the asymmetry parameter (usually small), and Q is the ^{57}Fe nuclear quadrupole moment, determined to be 0.16 barn (1 barn = 10^{-28} m^2) [73]. The EFG and asymmetry parameter are computed using the WIEN2K code [74], which adopts the augmented plane-wave plus local orbitals (APW + lo) method [75]. Given that $Q = 0.16$ barn is sometimes considered underestimated, we also use $Q = 0.18$ barn to compute the upper limit of QS.

III. RESULTS AND DISCUSSION

A. IS Fe^{2+} in ferropericlase

In Fp, Fe^{2+} substitutes Mg^{2+} in the MgO rocksalt structure, residing in an octahedral site surrounded by six oxygen atoms. For a d^6 ion (e.g., Fe^{2+}, Co^{3+}, ...) in such an octahedral site, there can be only one HS ($t_{2g}^4 e_g^2$) state and one LS ($t_{2g}^6 e_g^0$) state. The IS ($t_{2g}^5 e_g^1$) state, however, is not unique. A $t_{2g}^5 e_g^1$ state has a spin-down hole opened in the t_{2g} manifold. By properly choosing the coordinate system, this empty t_{2g} orbital can always be d_{xy}. The one filled spin-up e_g orbital can be either $d_{x^2-y^2}$ or d_{z^2}, forming two distinct IS states. Characterized by their filled e_g orbitals, these two IS states are referred to as the IS($x^2 - y^2$) and IS(z^2) state, respectively, as shown in Fig. 1. Since these two possible IS states have different Jahn-Teller (J-T) active orbitals occupied, their J-T distortions should be different as well: The IS($x^2 - y^2$) state would have elongated bond length on the xy plane, while the IS(z^2) state would have elongated bond length along the z direction.

Using the LDA + U method, all the above-mentioned spin states can be obtained in Fp. The U_{sc}'s of these states at different 64-atom $Mg_{1-x}Fe_xO$ ($x = 3.125\%$) supercell volumes are shown in Fig. 2. In Fp, the U_{sc} decreases with total electron spin S, similar to Fe-Pv [33], Fe-Ppv [39,40], and $LaCoO_3$ [64]. Another common feature shared by these systems is that the volume dependence of U_{sc} is marginal [33,39,40,64,76]. Notably, the U_{sc}'s of the two IS states are different, regardless of their same total spin moment $S = 1$. The U_{sc} of the IS(z^2) state is higher than that of the IS($x^2 - y^2$) state by 0.3–0.5 eV, indicating the former has a stronger on-site Coulomb interaction. It should be pointed out that the general trend of Hubbard U decreasing with total electron spin S was not observed in an earlier calculation on Fp [6]. The main reason is that the U_{sc}'s reported here are extracted from a series of
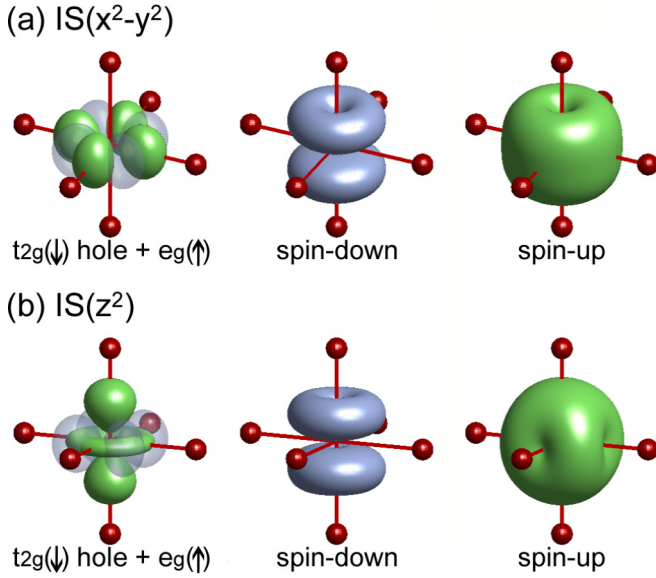
FIG. 1. (Color online) Possible electronic configurations of an intermediate-spin d^6 ion in a tetragonally distorted octahedral site. Schematic plots of the combination of t_{2g} hole (transparent blue) and filled e_g orbital (solid green), along with the spin-up/down electron density are shown. (a) The IS($x^2 - y^2$) state: a spin-down t_{2g} hole opened in the d_{xy} orbital and the spin-up e_g electron occupying the $d_{x^2-y^2}$ orbital. (b) The IS(z^2) state: a spin-down d_{xy} hole and a spin-up d_{z^2} electron.

trial LDA + U ground states, while the Hubbard U's reported in Ref. [6] were extracted from the LDA ground state. For the LS state in Fp, both LDA and LDA + U methods give an insulating ground state with the same orbital occupancy; the Hubbard U extracted from the LDA or LDA + U ground states are thus similar. For the HS state in Fp, however, LDA does not give a correct orbital occupancy; it gives three partially (and equally) occupied t_{2g} orbitals by one spin-down electron, resulting in a metallic state, in contrast with the LDA + U
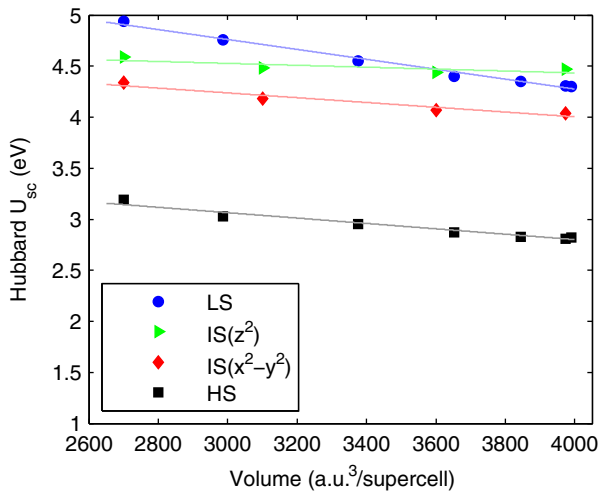

FIG. 2. (Color online) The self-consistent U (U_{sc}) of Fe^{2+} in (Mg$_{1-x}$,Fe$_x$)O ($x = 0.031\,25$) at different 64-atom supercell volumes (V) in the pressure range of 0–150 GPa (symbols). A straight line provides an adequate fit for $U_{sc}(V)$.

insulating ground state with one fully occupied t_{2g} orbital by one spin-down electron. The Hubbard U of HS Fe^{2+} in Fp reported in Ref. [6] is thus significantly different from the U_{sc} reported here.

The electronic structures and local Fe-O configurations of the two IS states at 112 GPa are shown in Fig. 3. The projected density of states (PDOS) of each cubic harmonic clearly shows that the IS($x^2 - y^2$) state has a filled spin-up $d_{x^2-y^2}$ orbital [Fig. 3(b)], and the IS(z^2) state has a filled spin-up d_{z^2} orbital [Fig. 3(e)]. The integrated local density of states (ILDOS) of all the Fe peaks in Figs. 3(a) and 3(d) are plotted in Figs. 3(c) and 3(f), respectively. These calculation results are consistent with the schematic plots shown in Fig. 1. By comparing Figs. 1(a) and 3(c), the IS($x^2 - y^2$) state shows a clear $t_{2g} + d_{x^2-y^2}$ character in its spin-up channel (an empty d_{z^2} orbital can be observed); by comparing Figs. 1(b) and 3(f), the IS(z^2) state shows a clear $t_{2g} + d_{z^2}$ character (an empty $d_{x^2-y^2}$ orbital can be observed). As expected, these two IS states exhibit distinct J-T distortions: the IS($x^2 - y^2$) state has elongated Fe-O distances on the xy plane [Fig. 3(c)], while the IS(z^2) state has elongated Fe-O distances along the z axis [Fig. 3(f)].

With the orbital occupancy and charge density shown above, the U_{sc}'s difference between the two IS states in Fp can be qualitatively explained. Indeed, our discussion is based on Kohn-Sham orbitals, which are usually considered of little physical meaning. In practice, however, they resemble the real electronic structure of most systems and can be used for molecular orbital or chemical analysis [77]. For the IS(z^2) state, its filled e_g orbital (d_{z^2}) is oriented vertically with the spin-down t_{2g} hole (d_{xy}) and *passing through* the donut-shape lobes of the spin-down electron charge density, as can be observed in Fig. 1(b). In contrast, the IS($x^2 - y^2$) state has its filled e_g orbital ($d_{x^2-y^2}$) oriented on the same plane with the spin-down t_{2g} hole, *laying in between* the donut-shape lobes of the spin-down electrons, as can be observed in Fig. 1(a). Clearly, the e_g electron of the IS(z^2) state overlaps with the spin-down electrons more than that in the IS($x^2 - y^2$) state. This greater electron-electron overlap in the IS(z^2) state leads to a stronger on-site Coulomb interaction and thus a higher U_{sc}.

One reliable way to identify iron spin state in Earth minerals is by comparing the iron nuclear QS obtained by theory and experiments, as demonstrated previously in Fe-Pv/Ppv [32,33,39,40]. The same approach can be applied to Fp as well. For each spin state, we compute the lower and upper limits of iron nuclear QS in the lower-mantle pressure range (see Sec. II). The calculation results are shown in Fig. 4(a), along with the measured QS (via Mössbauer spectroscopy) by Speziale *et al.* [4] and Kantor *et al.* [11] shown in Fig. 4(b). The dependence of QS on spin state can be understood via the electric field gradient, V_{zz}, at the iron nucleus. The QS is directly proportional to the EFG magnitude ($|V_{zz}|$), as shown in Eq. (1), and the d electrons contribute to the EFG as the following:

$$V_{zz} \propto \sum_\sigma \left(2n^\sigma_{x^2-y^2} - 2n^\sigma_{z^2} + 2n^\sigma_{xy} - n^\sigma_{yz} - n^\sigma_{xz}\right)/\langle r^3\rangle, \quad (2)$$

where $n^\sigma_{xy}, n^\sigma_{yz}, \ldots$ are the occupancy of each $3d$ orbital by the electron with spin σ [up ($\uparrow$) or down ($\downarrow$)]. Clearly, the dependence of QS on iron spin state results from the
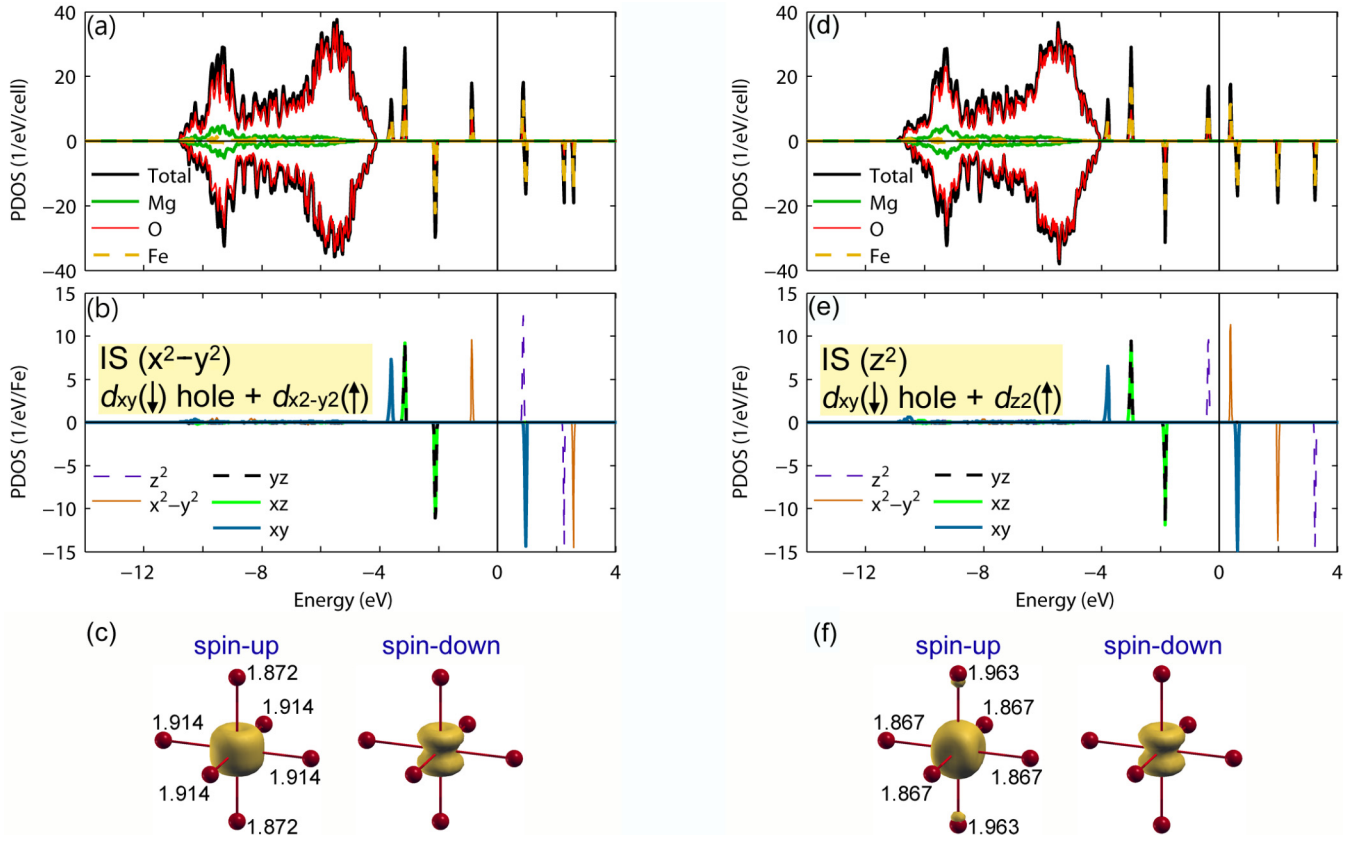
FIG. 3. (Color online) Electronic structures of the IS($x^2 - y^2$) state (a)–(c) and the IS(z^2) states (d)–(f) in (Mg$_{1-x}$,Fe$_x$)O ($x = 0.03125$) at 112 GPa. (a),(d) PDOS decomposed by atomic species. (b),(e) PDOS decomposed by cubic harmonic. (c),(f) The FeO$_6$ octahedron and ILDOS of Fe peaks shown in panels (a) and (d). Numbers in panels (c) and (f) indicate the Fe-O distances (in Å).

dependence of EFG on orbital occupancy, therefore, iron spin state cannot be directly derived from the numerical value of QS. In Fp, LS Fe^{2+} resides in an octahedral site with cubic (O_h) symmetry and has $n_{xy}^\sigma = n_{yz}^\sigma = n_{xz}^\sigma \approx 1$ and $n_{x^2-y^2}^\sigma = n_{z^2}^\sigma \approx 0$
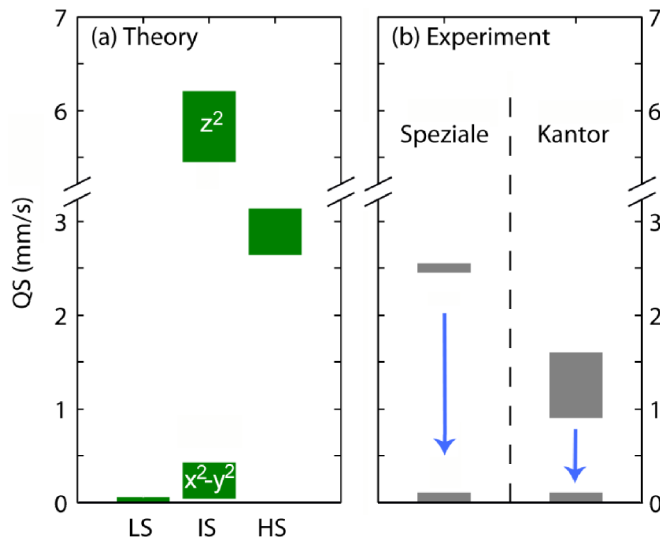

FIG. 4. (Color online) Calculated iron nuclear QS in ferroperi-clase (a) and experimental values (b) by Speziale *at al.* [4] and Kantor *et al.* [11]. Arrows in panel (b) indicate the drastic change in QS with increasing pressure.

for both spin up ($\sigma = \uparrow$) and spin down ($\sigma = \downarrow$). Its QS, based on Eq. (2), should be zero, consistent with Fig. 4(a). The HS Fe^{2+} has five spin-up electrons ($\sigma = \uparrow$) occupying all $3d$ orbitals forming a spherical shaped charge density. Evident from Eq. (2), these spin-up electrons barely contribute to the EFG. It is the one spin-down ($\sigma = \downarrow$) electron, d_{xy}, that contributes to the EFG. The computed QS of the HS state is about 2.6–3.1 mm/s, similar to that reported in Ref. [4], but higher than that reported in Ref. [11] [Fig. 4(b)]. The IS($x^2 - y^2$) state has $n_{x^2-y^2}^\uparrow \approx n_{xy}^\uparrow \approx n_{yz}^\uparrow \approx n_{xz}^\uparrow \approx 1$, $n_{xz}^\downarrow \approx n_{yz}^\downarrow \approx 1$, and the remaining orbitals being empty. Such a configuration, based on Eq. (2), would lead to an almost vanishing EFG and thus a very small QS. In contrast, the IS(z^2) state has $n_{z^2}^\uparrow \approx n_{xy}^\uparrow \approx n_{yz}^\uparrow \approx n_{xz}^\uparrow \approx 1$ and $n_{xz}^\downarrow \approx n_{yz}^\downarrow \approx 1$. This would lead to an EFG twice larger (in magnitude) than that of the HS state. Indeed, the computed QS of the IS(z^2) state is 5.5–6.2 mm/s. Such an exceptionally high QS is not observed in Fp. In this sense, the possibility of HS-IS(z^2)-LS crossover can be ruled out. While the remaining possible scenarios, HS-LS and HS-IS($x^2 - y^2$)-LS crossovers, are both consistent with Mössbauer spectra, first-principles calculations can provide further information to pin down the spin-crossover mechanism, as described below.

Using the LDA + U_{sc} method, the equations of state and energetics of (Mg$_{1-x}$,Fe$_x$)O ($x = 3.125\%$) in all spin states can be computed; the relative enthalpy (ΔH_i) of each spin state i [$i =$ HS, IS($x^2 - y^2$), IS(z^2), or LS] with respect to the
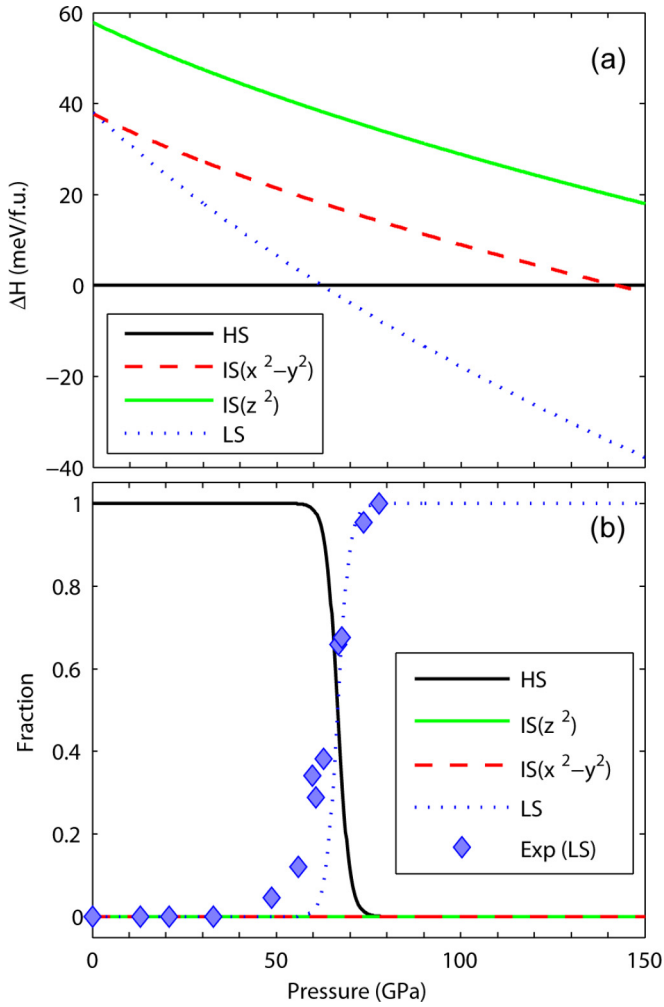
FIG. 5. (Color online) (a) Relative enthalpy (ΔH) of $(Mg_{1-x},Fe_x)O$ $(x = 0.031\,25)$ in each spin state with respect to the HS state. (b) Molar fraction of each spin state at room temperature predicted by theory (lines) and the LS fraction extracted from the Mössbauer spectra $(x = 0.05$ in the sample) [11].

HS state are plotted in Fig. 5(a). With known ΔH_i, the fraction (n_i) of each spin state can be estimated using the following expression derived from a thermodynamic model detailed in Refs. [30] and [36], subject to the constraint $\sum_i n_i = 1$,

$$n_i(P,T) = n_{HS} \frac{m_i(2S_i + 1)}{m_{HS}(2S_{HS} + 1)} \exp\left(-\frac{\Delta H_i}{k_B T x}\right)$$
$$\text{for } i \neq HS, \tag{3}$$

where m_i and S_i are the orbital degeneracy and total spin moment of spin state i, respectively. In Fp, $m_{HS} = m_{IS} = 3$ (for both types of IS), and $m_{LS} = 1$. The fraction n_i of each spin state at room temperature $(T = 300$ K) is plotted in Fig. 5(b). Here, we do not include vibrational free energy, as it only slightly increases the transition pressure [12,13] and would not change the main conclusion: Populations of the IS states are too low to be observed due to their extremely high enthalpies. This result is consistent with the lack of a QS of 5.5–6.2 mm/s in Mössbauer spectra; it also confirms the small QS observed in Fp should be the LS, not the IS$(x^2 - y^2)$ state,

showing that Fp undergoes a HS-LS crossover. We can also observe in Fig. 5(b) that overall, the computed LS fraction agrees very well with that derived from Mössbauer spectra of a sample with iron concentration $x = 0.05$ [11]. The small discrepancy is that in experiment, the LS fraction (n_{LS}) reaches 10% at ~ 55 GPa, while our calculation predicts ~ 62 GPa. Indeed, the transition pressure predicted by LDA + U_{sc} is slightly higher than that observed in Ref. [11] and other works comprehensively reviewed in Ref. [38]. Such a discrepancy may be better addressed by including the exchange term J computed self-consistently [71]. The HS state has a larger J than the LS state, which would increase the enthalpy of the HS state more, lower the relative enthalpy of the LS state (ΔH_{LS}), and thus lower the transition pressure.

While both IS states in Fp are unfavorable, a further analysis of this simple system can help us better understand IS Fe^{2+} in more complicated environments, including $(Mg,Fe)SiO_3$ Pv and Ppv. For Fe^{2+} (or any d^6 ion) in an octahedral site, an IS state can be produced from the LS state by opening a spin-down t_{2g} hole and filling a spin-up electron in an e_g orbital. We have shown that there can be more than one possible combination of t_{2g} hole and e_g electron (referred to as hole-electron combination hereafter). Furthermore, we shall see that among the possible IS states, the one with a closely oriented hole-electron combination has lower enthalpy, making it the *most probable* IS state. In Fp, the IS$(x^2 - y^2)$ state is the most probable IS state. Its filled e_g orbital, $d_{x^2-y^2}$, is closely oriented with its t_{2g} hole, d_{xy} ($d_{x^2-y^2}$ is simply a rotation with respect to d_{xy} about the z axis). Such a combination leads to a smaller overlap between the spin-up e_g electron and spin-down electrons and thus leads to a less strong on-site Coulomb interaction, smaller U_{sc} (as described previously), and a lower total energy. In contrast, the filled e_g orbital of the IS(z^2) state, d_{z^2}, is vertically oriented with the t_{2g} hole, d_{xy}. The overlap between its spin-up e_g electron and spin-down electrons, the on-site Coulomb interaction, and the totally energy are all larger.

Another attribute of the most probable IS Fe^{2+} is its lower QS compared with other possible IS states. This is also a consequence of the closely orientated hole and electron. For example, the IS$(x^2 - y^2)$ state has a $d_{x^2-y^2}$ electron and a d_{xy} hole. Evident from Eq. (2), $d_{x^2-y^2}$ and d_{xy} contribute equally to V_{zz}. Since the $d_{x^2-y^2}$ orbital is produced by a rotation of the d_{xy} orbital about the z axis, they should both have the same second derivative along the z direction. Starting with an LS state, opening a d_{xy} hole followed by filling a $d_{x^2-y^2}$ electron would not significantly change the EFG. Therefore, the QS of the IS$(x^2 - y^2)$ state should be very similar to that of the LS state. In contrast, the IS(z^2) is configured by opening a hole in d_{xy} of a LS state, followed by filling an electron in d_{z^2}, vertically oriented to d_{xy}. This would severely change the EFG and lead to a very different QS from the LS state. Based on this analysis, an IS Fe^{2+} (or d^6 ion) in a more complicated crystal-field environment could still have its energy lowered by bringing the hole-electron combination to a close configuration as in d_{xy}-$d_{x^2-y^2}$ that leads to a low QS.

B. IS Fe^{2+} in $MgSiO_3$ perovskite and postperovskite

As mentioned in Sec. I, first-principles computations so far do not support HS-IS crossover of Fe^{2+} in $(Mg,Fe)SiO_3$ Pv

but point to a crossover between two HS states with distinct QSs instead [32,33]. The finding of two distinct types of IS Fe^{2+} in Fp, however, suggests that further investigations, in particular, a thorough search for IS Fe^{2+} in Pv, would be necessary. Such a search, however, is not as straightforward as in Fp, as the atomic structure of Pv is more complicated, and the orbital occupancies of IS Fe^{2+} in Pv are not known *a priori*. To make sure all possible orbital occupancies are investigated, we produce IS Fe^{2+} by manipulating the orbital occupancy of LS Fe^{2+}. The reason is that LS and IS Fe^{2+} both displace from the high-symmetry mirror plane (in contrast to HS Fe^{2+}) to a position where only six oxygens are close enough to significantly affect the iron $3d$ electrons, namely, both LS and IS Fe^{2+} reside in a highly distorted octahedral crystal site [30]. As a consequence, the LS Fe^{2+} has three doubly occupied t_{2g}-like and two empty e_g-like orbitals [27]. An IS state can thus be produced by opening a spin-down hole in a t_{2g}-like orbital, filling a spin-up electron in an e_g-like orbital, followed by a structural optimization. Given the lack of symmetry in the distorted octahedral site, there are six possible hole-electron combinations to be tested (three inequivalent t_{2g}-like holes and two e_g-like orbitals), in contrast to two in Fp, where only tetragonal distortions are allowed. Among these six hole-electron combinations, only two can be stabilized. Characterized by their filled e_g-like orbitals, these two states are referred to as the $IS(z_L^2)$ and $IS(x_L^2 - y_L^2)$ states, respectively, and they both have a U_{sc} of 4.3 eV. As shall be detailed below, however, these IS states are not exactly the same as those in Fp. With different orbital occupancies, the position of these two IS Fe^{2+} in the big cage and the local Fe-O configurations are different. Their atomic structures at 120 GPa are shown in Fig. 6, where the numbers in panels (b) and (d) are the Fe-O distances (in Å). For each case, a local coordinate system (x_L, y_L, z_L) based on the Fe-O bonds can be defined, and it does not align with the crystallographic coordinates $(\mathbf{a}, \mathbf{b}, \mathbf{c})$. In such a highly distorted octahedral crystal field, the d orbitals would no longer be cubic harmonics.

Among the two IS states, the $IS(z_L^2)$ state is briefly reported in Ref. [32] without insightful analysis. The PDOS of this state at 120 GPa is shown in Fig. 7(a), where the peaks (indicated by letters b–f) resulting from iron $3d$ electrons can be clearly observed. The ILDOS of each peak are plotted in Figs. 7(b)–7(f), respectively. The lowest three orbitals (b, c, and d) exhibit t_{2g} character. In terms of the locally defined Fe-O coordinate (x_L, y_L, z_L), these three orbitals are $\sim d_{x_L y_L}$, $\sim (d_{x_L z_L} - d_{y_L z_L})/\sqrt{2}$, and $\sim (d_{x_L z_L} + d_{y_L z_L})/\sqrt{2}$, respectively. The other two orbitals (e and f) exhibit e_g characters; they are $\sim d_{z_L^2}$ and $\sim d_{x_L^2 - y_L^2}$, respectively. The filled e_g-like orbital, $\sim d_{z_L^2}$, is consistent with the longer Fe-O distance in the z_L direction [Fig. 6(b)]. In this state, the spin-down hole is opened in the $\sim (d_{x_L z_L} + d_{y_L z_L})/\sqrt{2}$ orbital, closely oriented with the $\sim d_{z_L^2}$ orbital. Such a hole-electron combination is schematically depicted in Fig. 7(g). As can be observed, the filled e_g-like orbital of this state is almost a rotation with respect to the t_{2g}-like hole. In this sense, this state is more similar to the $IS(x^2 - y^2)$ state in Fp, rather than the $IS(z^2)$ in Fp. Therefore, the QS of this state is quite low, about 0.9–1.6 mm/s (depending on pressure), slightly higher than the QS of LS Fe^{2+} in Pv, 0.8 mm/s [32,33]. The PDOS of the $IS(x_L^2 - y_L^2)$ state is shown in Fig. 7(h). The ILDOS of
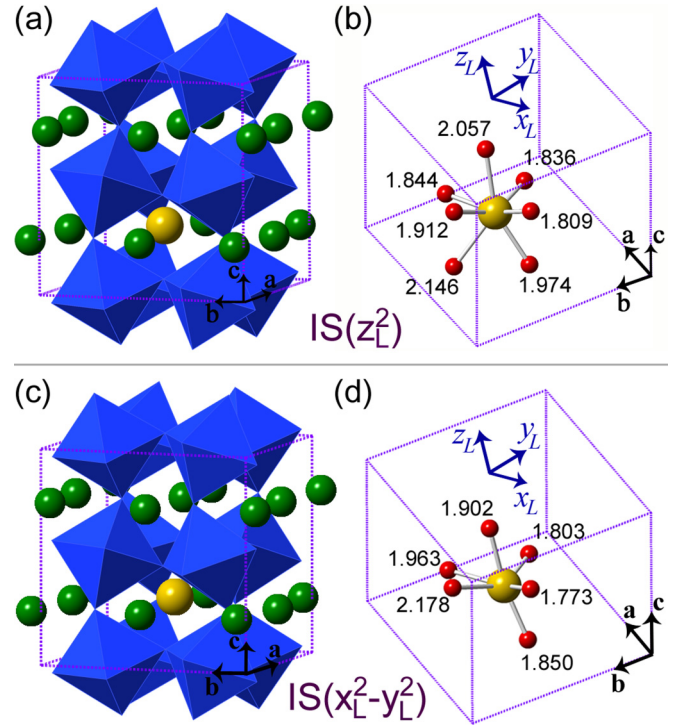

FIG. 6. (Color online) Atomic structure [(a),(c)] and the local Fe-O configuration [(b),(d)] of $(Mg_{1-x}, Fe_x)SiO_3$ perovskite ($x = 0.125$) with $IS(z_L^2)$ and $IS(x_L^2 - y_L^2)$ Fe^{2+} at 120 GPa. The large (yellow), medium (green), and small (red) spheres are Fe, Mg, and O atoms, respectively; the octahedra (blue) are SiO_6 octahedra. The dotted (purple) line indicates the 40-atom supercell. Numbers in panels (b) and (d) indicate the Fe-O distances (in Å). A set of Fe-O local coordinates (x_L, y_L, z_L) can be defined, and they do not align with the crystallographic coordinates $(\mathbf{a}, \mathbf{b}, \mathbf{c})$.

each peak (i–m) resulting from iron $3d$ electrons are shown in Figs. 7(i)–7(m), respectively. The lowest three orbitals (i, j, and k) exhibit t_{2g} characters: $\sim d_{y_L z_L}$, $\sim d_{x_L z_L}$, and $\sim d_{x_L y_L}$, respectively. The filled e_g-like orbital is $\sim d_{x^2 - y^2}$, consistent with the longer average Fe-O distances on the $x_L y_L$ plane [Fig. 6(d)]. This state has a hole in the $\sim d_{x_L y_L}$ orbital; it resembles the $IS(x^2 - y^2)$ state in Fp. As expected, it has quite low QS, 0.8–1.4 mm/s (depending on pressure), which is in between the QSs of the LS and $IS(z^2)$ state in Pv.

To determine whether IS Fe^{2+} in Pv is possible at all, we compute the enthalpy of all possible spin states, including the two HS states with distinct QSs (referred to as low-QS and high-QS HS states) reported in Refs. [32] and [33], the two IS states, and one LS state. The relative enthalpy of these states with respect to the high-QS HS state, along with the computed QSs, are shown in Fig. 8 (QSs of HS states are adopted from Ref. [33]). The U_{sc} of the HS and LS Fe^{2+} are 3.1 and 4.5 eV, respectively, nearly the same as those reported in Ref. [32], which extracts U from the DFT ground states. The reason is that for (Mg,Fe)SiO_3 Pv with low iron concentration, standard DFT functionals can give correct insulating state and orbital occupancy for the HS and LS states; extracting U from DFT or DFT + U ground states should thus give similar results. Also, the U_{sc} of Fe^{2+} in Pv barely depends on supercell volume and can be treated as a constant with
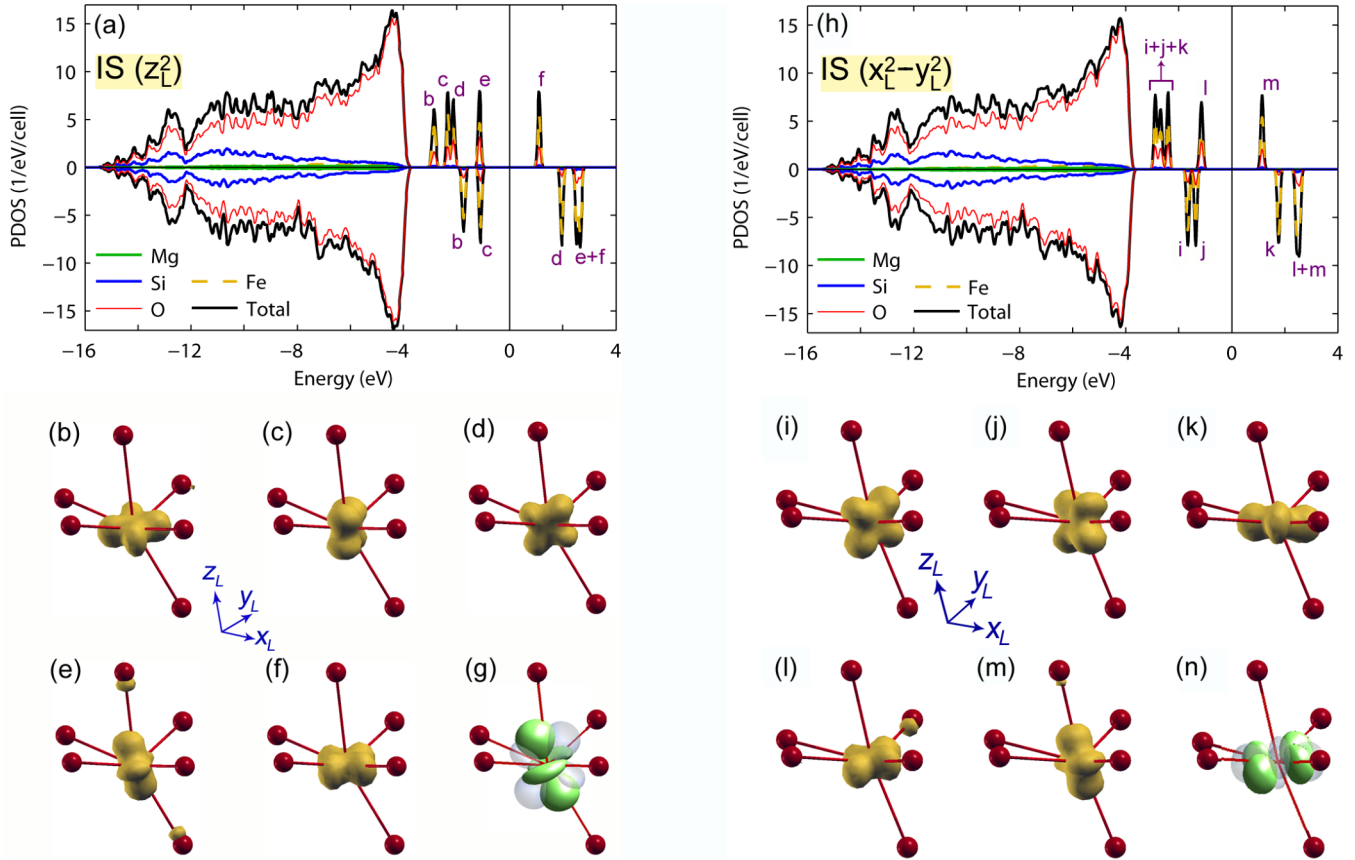
FIG. 7. (Color online) Electronic structure of IS(z_L^2) state [(a)–(g)] and IS($x_L^2 - y_L^2$) state [(h)–(n)] of $(Mg_{1-x},Fe_x)SiO_3$ perovskite ($x = 0.125$) at 120 GPa. (a),(h) PDOS decomposed by atomic species, where peaks b–f and i–m are contributed by iron, and each of their ILDOS are plotted in panels (b)–(f) and (i)–(m), respectively. The Fe-O distorted octahedra are the same as in Figs. 6(b) and 6(d), with the longest Fe-O (2.146 Å) in 6(b) omitted. Panels (b)–(d) and (i)–(k) exhibit t_{2g} character, while panels (e)–(f) and (l)–(m) exhibit e_g character. The IS(z_L^2) state has a t_{2g}-like hole opened in the $\sim (d_{x_L z_L} + d_{y_L z_L})/\sqrt{2}$ orbital (d) and an e_g-like electron occupying the $\sim d_{z_L^2}$ orbital (e). The IS($x_L^2 - x_L^2$) state has a t_{2g}-like hole opened in the $\sim (d_{x_L y_L})$ orbital (k) and an e_g-like electron occupying the $\sim d_{x_L^2 - y_L^2}$ orbital (l). The hole-electron combinations of these two states are schematically depicted in panels (g) and (n), where the transparent (gray) and solid (green) surfaces indicate the hole and the electron, respectively.

respect to volume. Evident from Fig. 8, the two IS states are energetically competitive. In 0–32 GPa, the IS($x_L^2 - y_L^2$) state has lower enthalpy; in 32–150 GPa, which covers most of the lower-mantle pressure range, the IS(z_L^2) has lower enthalpy, making it the most probable IS state in the lower mantle. The reason why these two IS states have similar physical properties (QS, U_{sc}, and enthalpy) is that the IS(z_L^2) state in Pv has its t_{2g} hole in the $(d_{x_L z_L} + d_{y_L z_L})/\sqrt{2}$ orbital, closely oriented with the $d_{z_L^2}$ orbital, instead of in the $d_{x_L y_L}$ orbital. Hypothetically, if the t_{2g}-like hole of the IS(z_L^2) state in Pv were opened in the $d_{x_L y_L}$ orbital like the IS(z^2) state in Fp, the on-site Coulomb interaction would be stronger, the self-consistent Hubbard U_{sc} would be larger, the total energy would be significantly higher, and the QS would be exceptionally large. To reduce the energy, both IS states in (Mg,Fe)SiO$_3$ Pv have closely oriented hole-electron combination, similar to the IS($x^2 - y^2$) state in Fp. Regardless, these two IS states are still not favorable. The only crossover in this system occurs between the low-QS and high-QS HS states at 20 GPa, similar to the previous calculation [32].

As shown above, IS Fe^{2+} in (Mg,Fe)SiO$_3$ Pv resides in a distorted octahedral crystal field, with orbitals exhibiting t_{2g} and e_g characters. With one e_g-like orbital being filled, the t_{2g}-like hole is uniquely determined as well: It should be opened in the most closely oriented orbital to reduce the total energy. Given that there are only two e_g-like orbitals, the two IS states reported here should include all possible IS Fe^{2+} in Pv. The signature of IS Fe^{2+} in Pv in the lower-mantle pressure range should be a QS in between 0.8 and 1.6 mm/s. Given the lack of such QS observed in the Mössbauer spectra and the high enthalpy of IS state, the observed QS (3.5 mm/s [28]) should be indeed a HS state, and IS Fe^{2+} in Pv would be highly unlikely.

While a similar investigation for Fe-Ppv is not conducted here, an IS Fe^{2+} in Ppv has been reported in Ref. [39], and it is similar to the IS(z_L^2) state in Pv. Given the highly similar crystal fields experienced by Fe^{2+} in Pv and Ppv, this reported IS state in Ppv should be the most probable IS state in the D'' pressure range, if not only. Nevertheless, this IS state is still unfavorable, and its QS is inconsistent with experiments, as
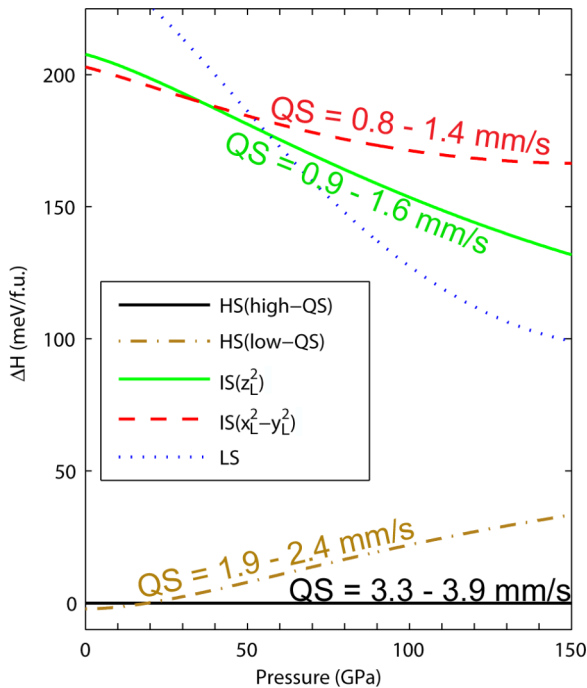
FIG. 8. (Color online) Relative enthalpy (ΔH) of $(Mg_{1-x},Fe_x)SiO_3$ perovskite $(x = 0.125)$ in each spin state with respect to the high-QS HS state. The QSs of HS states adopted from Ref. [33]. As indicated, a QS of 3.5 mm/s is *not* a signature of IS Fe^{2+}.

detailed in Ref. [39]. Therefore, IS Fe^{2+} in Ppv should also be highly unlikely.

IV. CONCLUSION

Using LDA $+ U_{sc}$ calculations, we have investigated in detail the possible stability of the controversial intermediate-spin state of Fe^{2+} in lower-mantle minerals subject to pressure-induced spin crossover: ferropericlase $[(Mg_{1-x},Fe_x)O]$ $(x = 0.031\,25)$ and $(Mg_{1-x},Fe_x)SiO_3$ perovskite $(x = 0.125)$. Two types of IS states with distinct $3d$ hole-electron combinations were found in Fp: the IS$(x^2 - y^2)$ state and the IS(z^2) state, with a $d_{x^2-y^2}$ and d_{z^2} electron, respectively, and a d_{xy} hole. These distinct orbital occupancies lead to distinct Jahn-Teller distortions and iron nuclear quadrupole splittings: The IS(z^2)

state has an exceptionally high QS $(\geqslant 5.5$ mm/s$)$, and the IS$(x^2 - y^2)$ state has a quite low QS $(< 0.5$ mm/s$)$. The on-site Coulomb interaction and the total energy of the IS$(x^2 - y^2)$ state are both lower than that of the IS(z^2) state because of its closely oriented hole-electron combination, namely, less overlap between the spin-up e_g and spin-down t_{2g} electrons. In $(Mg,Fe)SiO_3$ Pv, although IS Fe^{2+} resides in the large dodecahedral site, it effectively experiences a distorted octahedral crystal field. Two types of IS states are found, and they can also be characterized by their filled e_g-like orbitals. The hole-electron combinations of these two IS states are both closely oriented; they both exhibit characters similar to the IS$(x^2 - y^2)$ state in Fp. Therefore, these two IS Fe^{2+} in Pv have similarly low QS $(< 1.6$ mm/s$)$ and the same Hubbard U_{sc}, and they are energetically competitive. Compared to the HS and LS states, all the above-mentioned IS states in Fp and $(Mg,Fe)SiO_3$ Pv/Ppv are energetically unfavorable; their QSs are also all inconsistent with experiments. Most importantly, these considered IS Fe^{2+} already include all relevant types of IS Fe^{2+} in lower-mantle minerals. Therefore, it is highly unlikely that IS Fe^{2+} exists in the lower mantle.

Finally, although this present work is mainly focused on lower-mantle minerals under pressure (variable metal-oxygen distance), it is an exemplar of the behavior of other strongly correlated d^6 ions in two common crystalline sites of complex oxides: the octahedral (B) site in ABO_3 perovskite and in the rocksalt structure, and the dodecohedral (A) site in perovskites. Present results and conclusions could be applicable to or serve as a starting point of investigation for several equivalent problems where the roles played by chemical variation or thermal expansion/contraction can be seen as analogous to pressure, as with spin excitation in rare-earth cobaltites at finite (but low) temperatures.

[1] J. Badro, G. Fiquet, F. Guyot, J. Rueff, V. Struzhkin, G. Vanko, and G. Monaco, Science **300**, 789 (2003).

[2] J. Badro, J. Rueff, G. Vanko, G. Monaco, G. Fiquet, and F. Guyot, Science **305**, 383 (2004).

[3] J.-F. Lin, V. V. Struzhkin, S. D. Jacobsen, M. Y. Hu, P. Chow, J. Kung, H. Liu, H.-k. Mao, and R. J. Hemley, Nature (London) **436**, 377 (2005).

[4] S. Speziale, A. Milber, V. E. Lee, S. M. Clark, M. P. Pasternak, and R. Jeanloz, Proc. Natl. Acad. Sci. USA **102**, 17918 (2005).

[5] I. Y. Kantor, L. S. Dubrovinsky, and C. A. McCammon, Phys. Rev. B **73**, 100101(R) (2006).

[6] T. Tsuchiya, R. M. Wentzcovitch, C. R. S. da Silva, and S. de Gironcoli, Phys. Rev. Lett. **96**, 198501 (2006).

[7] A. F. Goncharov, V. V. Struzhkin, and S. D. Jacobsen, Science **312**, 1205 (2006).

[8] J.-F. Lin, G. Vanko, S. D. Jacobsen, V. Iota, V. V. Struzhkin, V. B. Prakapenka, A. Kuznetsov, and C.-S. Yoo, Science **317**, 1740 (2007).

[9] J. Crowhurst, J. M. Brown, A. F. Goncharov, and S. D. Jacobsen, Science **319**, 451 (2008).

[10] J.-F. Lin, S. T. Weir, D. D. Jackson, W. J. Evans, Y. K. Vohra, W. Qiu, and C.-S. Yoo, Geophys. Res. Lett. **34**, L16305 (2007).

[11] I. Kantor, L. Dubrovinsky, C. McCammon, G. Steinle-Neumann, A. Kantor, N. Skorodumova, S. Pascarelli, and G. Aquilanti, Phys. Rev. B **80**, 014204 (2009).

[12] Z. Wu, J. F. Justo, C. R. S. da Silva, S. de Gironcoli, and R. M. Wentzcovitch, Phys. Rev. B **80**, 014409 (2009).

[13] R. M. Wentzcovitch, J. F. Justo, Z. Wu, C. R. S. da Silva, D. A. Yuen, and D. Kohlstedtd, Proc. Natl. Acad. Sci. USA **106**, 8447 (2009).

[14] H. Marquardt, S. Speziale, H. J. Reichmann, D. J. Frost, F. R. Schilling, and E. J. Garnero, Science **324**, 224 (2009).

[15] D. Antonangeli, J. Siebert, C. M. Aracne, D. L. Farber, A. Bosak, M. Hoesch, M. Krisch, F. J. Ryerson, G. Fiquet, and J. Badro, Science **331**, 64 (2011).

[16] Z. Wu, J. F. Justo, and R. M. Wentzcovitch, Phys. Rev. Lett. **110**, 228501 (2013).

[17] S. Saha, A. Bengtson, K. L. Crispin, J. A. Van Orman, and D. Morgan, Phys. Rev. B **84**, 184102 (2011).

[18] M. W. Ammann, J. P. Brodholt, and D. P. Dobson, Earth Planet. Sci. Lett. **302**, 393 (2011).

[19] S. Saha, A. Bengtson, and D. Morgan, Earth Planet. Sci. Lett. **362**, 1 (2013).

[20] J. Li, V. V. Struzhkin, H.-k. Mao, J. Shu, R. J. Hemley, Y. Fei, B. Mysen, P. Dera, V. Prakapenka, and G. Shen, Proc. Natl. Acad. Sci. USA **101**, 14027 (2004).

[21] J. M. Jackson, W. Sturhahn, G. Shen, J. Zhao, M. Y. Hu, D. Errandonea, J. D. Bass, and Y. Fei, Am. Mineral. **90**, 199 (2005).

[22] J. Li, W. Sturhahn, J. M. Jackson, V. V. Struzhkin, J. F. Lin, J. Zhao, H. Mao, and G. Shen, Phys. Chem. Miner. **33**, 575 (2006).

[23] A. M. Hofmeister, Earth Planet. Sci. Lett. **243**, 44 (2006).

[24] F. Zhang and A. R. Oganov, Earth Planet. Sci. Lett. **249**, 436 (2006).

[25] S. Stackhouse, J. P. Brodholt, and G. D. Price, Earth Planet. Sci. Lett. **253**, 282 (2007).

[26] A. Bengtson, K. Persson, and D. Morgan, Earth Planet. Sci. Lett. **265**, 535 (2008).

[27] K. Umemoto, R. M. Wentzcovitch, Y. G. Yu, and R. Requis, Earth Planet. Sci. Lett. **276**, 198 (2008).

[28] C. McCammon, I. Kantor, O. Narygina, J. Rouquette, U. Ponkratz, I. Sergueev, M. Mezouar, V. Prakapenka, and L. Dubrovinsky, Nat. Geosci. **1**, 684 (2008).

[29] A. Bengtson, J. Li, and D. Morgan, Geophys. Res. Lett. **36**, L15301 (2009).

[30] K. Umemoto, H. Hsu, and R. M. Wentzcovitch, Phys. Earth Planet. Inter. **180**, 209 (2010).

[31] K. Catalli, S.-H. Shim, V. B. Prakapenka, J. Zhao, W. Sturhahn, P. Chow, Y. Xiao, H. Liu, H. Cynn, and W. J. Evans, Earth Planet. Sci. Lett. **289**, 68 (2010).

[32] H. Hsu, K. Umemoto, P. Blaha, and R. M. Wentzcovitch, Earth Planet. Sci. Lett. **294**, 19 (2010).

[33] H. Hsu, P. Blaha, M. Cococcioni, and R. M. Wentzcovitch, Phys. Rev. Lett. **106**, 118501 (2011).

[34] V. Potapkin, C. McCammon, K. Glazyrin, A. Kantor, I. Kupenko, C. Prescher, R. Sinmyo, G. V. Smirnov, A. I. Chumakov, R. Rüffer, and L. Dubrovinsky, Nat. Commun. **4**, 1427 (2013).

[35] J.-F. Lin and T. Tsuchiya, Phys. Earth Planet. Inter. **170**, 248 (2008).

[36] H. Hsu, K. Umemoto, Z. Wu, and R. M. Wentzcovitch, Rev. Mineral Geochem. **71**, 169 (2010).

[37] R. M. Wentzcovitch, H. Hsu, and K. Umemoto, Eur. J. Mineral. **24**, 851 (2012).

[38] J.-F. Lin, S. Speziale, Z. Mao, and H. Marquardt, Rev. Geophys. **51**, 244 (2013).

[39] Y. G. Yu, H. Hsu, M. Cococcioni, and R. M. Wentzcovitch, Earth Planet. Sci. Lett. **331–332**, 1 (2012).

[40] H. Hsu, Y. G. Yu, and R. M. Wentzcovitch, Earth Planet. Sci. Lett. **359–360**, 34 (2012).

[41] L. Zhang, Y. Meng, W. Yang, L. Wang, W. L. Mao, Q.-S. Zeng, J. S. Jeong, A. J. Wagner, K. A. Mkhoyan, W. Liu, R. Xu, and H.-k. Mao, Science **344**, 877 (2014).

[42] R. Larico, L. V. C. Assali, and J. F. Justo, Phys. Rev. B **87**, 165113 (2013).

[43] L. Hunter, J. Gordon, S. Peck, D. Ang, and J.-F. Lin, Science **339**, 928 (2013).

[44] F. Krüger, S. Kumar, J. Zaanen, and J. van den Brink, Phys. Rev. B **79**, 054504 (2009).

[45] V. Gnezdilov, Yu. Pashkevich, P. Lemmens, A. Gusev, K. Lamonova, T. Shevtsova, I. Vitebskiy, O. Afanasiev, S. Gnatchenko, V. Tsurkan, J. Deisenhofer, and A. Loidl, Phys. Rev. B **83**, 245127 (2011).

[46] R. Yu and Q. Si, Phys. Rev. B **84**, 235115 (2011).

[47] L. Simonelli, N. L. Saini, M. M. Sala, Y. Mizuguchi, Y. Takano, H. Takeya, T. Mizokawa, and G. Monaco, Phys. Rev. B **85**, 224510 (2012).

[48] *Spin Crossover in Transition Metal Compounds I–III*, edited by P. Gütlich and H. A. Goodwin, Topics in Current Chemistry Vols. 233–235 (Springer, New York, 2004).

[49] W. Zhang, R. Alonso-Mori, U. Bergmann, C. Bressler, M. Chollet, A. Galler, W. Gawelda, R. G. Hadt, R. W. Hartsock, T. Kroll, K. S. Kjr, K. Kubicek, H. T. Lemke, H. W. Liang, D. A. Meyer, M. M. Nielsen, C. Purser, J. S. Robinson, E. I. Solomon, Z. Sun, D. Sokaras, T. B. van Driel, G. Vanko, T.-C. Weng, D. Zhu, and K. J. Gaffney, Nature (London) **509**, 345 (2014).

[50] K. Tarafder, S. Kanungo, P. M. Oppeneer, and T. Saha-Dasgupta, Phys. Rev. Lett. **109**, 077203 (2012).

[51] D. Fuchs, C. Pinta, T. Schwarz, P. Schweiss, P. Nagel, S. Schuppler, R. Schneider, M. Merz, G. Roth, and H. v. Lohneysen, Phys. Rev. B **75**, 144402 (2007).

[52] D. Fuchs, E. Arac, C. Pinta, S. Schuppler, R. Schneider, and H. v. Lohneysen, Phys. Rev. B **77**, 014434 (2008).

[53] J. W. Freeland, J. X. Ma, and J. Shi, Appl. Phys. Lett. **93**, 212501 (2008).

[54] S. Park, P. Ryan, E. Karapetrova, J. W. Kim, J. X. Ma, J. Shi, J. W. Freeland, and W. Wu, Appl. Phys. Lett. **95**, 072508 (2009).

[55] A. Herklotz, A. D. Rata, L. Schultz, and K. Dorr, Phys. Rev. B **79**, 092409 (2009).

[56] V. V. Mehta, M. Liberati, F. J. Wong, R. V. Chopdekar, E. Arenholz, and Y. Suzuki, J. Appl. Phys. **105**, 07E503 (2009).

[57] M. Merz, P. Nagel, C. Pinta, A. Samartsev, H. v. Lhneysen, M. Wissinger, S. Uebe, A. Assmann, D. Fuchs, and S. Schuppler, Phys. Rev. B **82**, 174416 (2010).

[58] A. Posadas, M. Berg, H. Seo, A. de Lozanne, A. A. Demkov, D. J. Smith, A. P. Kirk, D. Zhernokletov, and R. M. Wallace, Appl. Phys. Lett. **98**, 053104 (2011).

[59] C. Pinta, D. Fuchs, M. Merz, M. Wissinger, E. Arac, H. v. Löhneysen, A. Samartsev, P. Nagel, and S. Schuppler, Phys. Rev. B **78**, 174402 (2008).

[60] D. Fuchs, L. Dieterle, E. Arac, R. Eder, P. Adelmann, V. Eyert, T. Kopp, R. Schneider, D. Gerthsen, and H. v. Löhneysen, Phys. Rev. B **79**, 024424 (2009).

[61] K. Gupta and P. Mahadevan, Phys. Rev. B **79**, 020406(R) (2009).

[62] J. M. Rondinelli and N. A. Spaldin, Phys. Rev. B **79**, 054409 (2009).

[63] H. Hsu, P. Blaha, R. M. Wentzcovitch, and C. Leighton, Phys. Rev. B **82**, 100406(R) (2010).

[64] H. Hsu, P. Blaha, and R. M. Wentzcovitch, Phys. Rev. B **85**, 140404(R) (2012).

[65] W. S. Choi, J.-H. Kwon, H. Jeen, J. E. Hamann-Borrero, A. Radi, S. Macke, R. Sutarto, F. He, G. A. Sawatzky, V. Hinkov, M. Kim, and H. N. Lee, Nano Lett. **12**, 4966 (2012).

[66] J. Fujioka, Y. Yamasaki, H. Nakao, R. Kumai, Y. Murakami, M. Nakamura, M. Kawasaki, and Y. Tokura, Phys. Rev. Lett. **111**, 027206 (2013).

[67] R. M. Wentzcovitch, J. L. Martins, and G. D. Price, Phys. Rev. Lett. **70**, 3947 (1993).

[68] P. Giannozzi, S. Baroni, N. Bonini, M. Calandra, R. Car, C. Cavazzoni, D. Ceresoli, G. L. Chiarotti, M. Cococcioni, I. Dabo, A. Dal Corso, S. de Gironcoli, S. Fabris, G. Fratesi, R. Gebauer, U. Gerstmann, C. Gougoussis, A. Kokalj, M. Lazzeri, Layla Martin-Samos, N. Marzari, F. Mauri, R. Mazzarello,

S. Paolini, A. Pasquarello, L. Paulatto, C. Sbraccia, S. Scandolo, G. Sclauzero, A. P. Seitsonen, A. Smogunov, P. Umari, and R. M. Wentzcovitch, J. Phys.: Condens. Matter **21**, 395502 (2009).

[69] H. J. Kulik, M. Cococcioni, D. A. Scherlis, and N. Marzari, Phys. Rev. Lett. **97**, 103001 (2006).

[70] V. L. Campo, Jr. and M. Cococcioni, J. Phys.: Condens. Matter **22**, 055602 (2010).

[71] B. Himmetoglu, R. M. Wentzcovitch, and M. Cococcioni, Phys. Rev. B **84**, 115108 (2011).

[72] M. Cococcioni and S. de Gironcoli, Phys. Rev. B **71**, 035105 (2005).

[73] H. M. Petrilli, P. E. Blochl, P. Blaha, and K. Schwarz, Phys. Rev. B **57**, 14690 (1998).

[74] P. Blaha, K. Schwarz, G. Madsen, D. Kvasnicka, and J. Luitz, *WIEN2k, An Augmented Plane Wave Plus Local Orbitals Program for Calculating Crystal Properties*, edited by K. Schwarz (Techn. Universität Wien, Vienna, 2001).

[75] G. K. H. Madsen, P. Blaha, K. Schwarz, E. Sjostedt, and L. Nordstrom, Phys. Rev. B **64**, 195134 (2001).

[76] H. Hsu, K. Umemoto, M. Cococcioni, and R. M. Wentzcovitch, Phys. Rev. B **79**, 125124 (2009).

[77] R. Stowasser and R. Hoffmann, J. Am. Chem. Soc. **121**, 3414 (1999).